ACSNANO
www.acsnano.org
ARTICLE

Protecting Silicon Film Anodes in Lithium-Ion Batteries Using an Atomically Thin Graphene Drape

Shravan Suresh,[†] Zi Ping Wu,[‡] Stephen F. Bartolucci,[§] Swastik Basu,[†] Rahul Mukherjee,[∥] Tushar Gupta,[†] Prateek Hundekar,[⊥] Yunfeng Shi,[⊥] Toh-Ming Lu,[#] and Nikhil Koratkar*[,†,⊥]

[†]Department of Mechanical, Aerospace and Nuclear Engineering, [⊥]Department of Material Science and Engineering, and [#]Department of Physics, Applied Physics and Astronomy, Rensselaer Polytechnic Institute, Troy, New York 12180, United States

[‡]Jiangxi Key Laboratory of Power Battery and Materials, School of Materials Science and Engineering, Jiangxi University of Science and Technology, Ganzhou 341000, People's Republic of China

[§]U.S. Army Armaments Research Development and Engineering Center, Benet Laboratories, Watervliet, New York 12189, United States

[∥]Enermat Technologies, Inc., Troy, New York, United States

Supporting Information

ABSTRACT: **Silicon (Si) shows promise as an anode material in lithium-ion batteries due to its very high specific capacity. However, Si is highly brittle, and in an effort to prevent Si from fracturing, the research community has migrated from the use of Si films to Si nanoparticle based electrodes. However, such a strategy significantly reduces volumetric energy density due to the porosity of Si nanoparticle electrodes. Here we show that contrary to conventional wisdom, Si films can be stabilized by two strategies: (a) anchoring the Si films to a carbon nanotube macrofilm (CNM) current collector and (b) draping the films with a graphene monolayer. After electrochemical cycling, the graphene-coated Si films on CNM resembled a tough mud-cracked surface in which the graphene capping layer suppresses delamination and stabilizes the solid electrolyte interface. The graphene-draped Si films on CNM exhibit long cycle life (>1000 charge/discharge steps) with an average specific capacity of ~806 mAh g^{-1}. The volumetric capacity averaged over 1000 cycles of charge/discharge is ~2821 mAh cm^{-3}, which is 2 to 5 times higher than what is reported in the literature for Si nanoparticle based electrodes. The graphene-draped Si anode could also be successfully cycled against commercial cathodes in a full-cell configuration.**

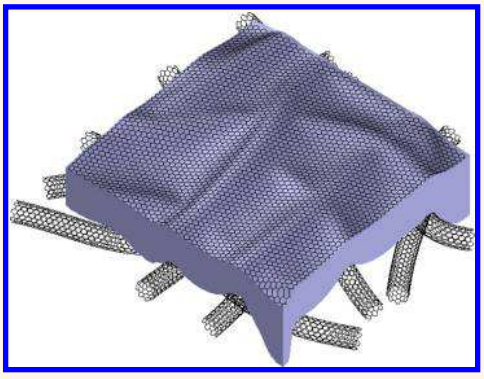

KEYWORDS: *silicon film anodes, monolayer graphene, graphene encapsulation, stable cycle life, volumetric energy density*

The energy storage industry is experiencing rapid growth and is expected to more than double in size over the next five years. Lithium (Li)-ion cell production has gone up from ~26 GWh in 2011 to over ~61 GWh in 2015 and is expected to grow to ~125 GWh by 2020.[1] This growth is led by the explosive use of consumer electronics with phones, tablets, and laptops proliferating as engines of our modern economy. In addition, about a third of current Li-ion demand is driven by the electrification of automobiles, with hybrids and electric vehicles taking a prominent place in our battle against greenhouse gas emissions.[2] Not only are Li-ion batteries deployed in consumer electronics and electric vehicles, they also service cutting-edge technologies in emergent segments such as grid storage, wearable consumer and military electronics, unmanned aerial vehicles, robotics and even spacesuits, planetary exploration probes, and satellites.[3] A number of the above applications impose demands on battery systems that current Li-ion cell chemistries are unable to satisfy, either on a performance or cost basis. Development of high energy density and long cycle life anode and cathode materials is therefore indispensable to keep pace with the rising demands of consumers.

Conventional lithium-ion batteries (LIBs) with graphite-based anodes display a theoretical gravimetric charge storage capacity of ~372 mAh g^{-1} based on the anode mass.[4] Silicon (Si) has been identified as a potential choice to replace traditional graphite, as its theoretical capacity (~4200 mAh g^{-1}

Received: March 14, 2017
Accepted: April 17, 2017
Published: April 17, 2017

DOI: 10.1021/acsnano.7b01780
ACS Nano 2017, 11, 5051−5061

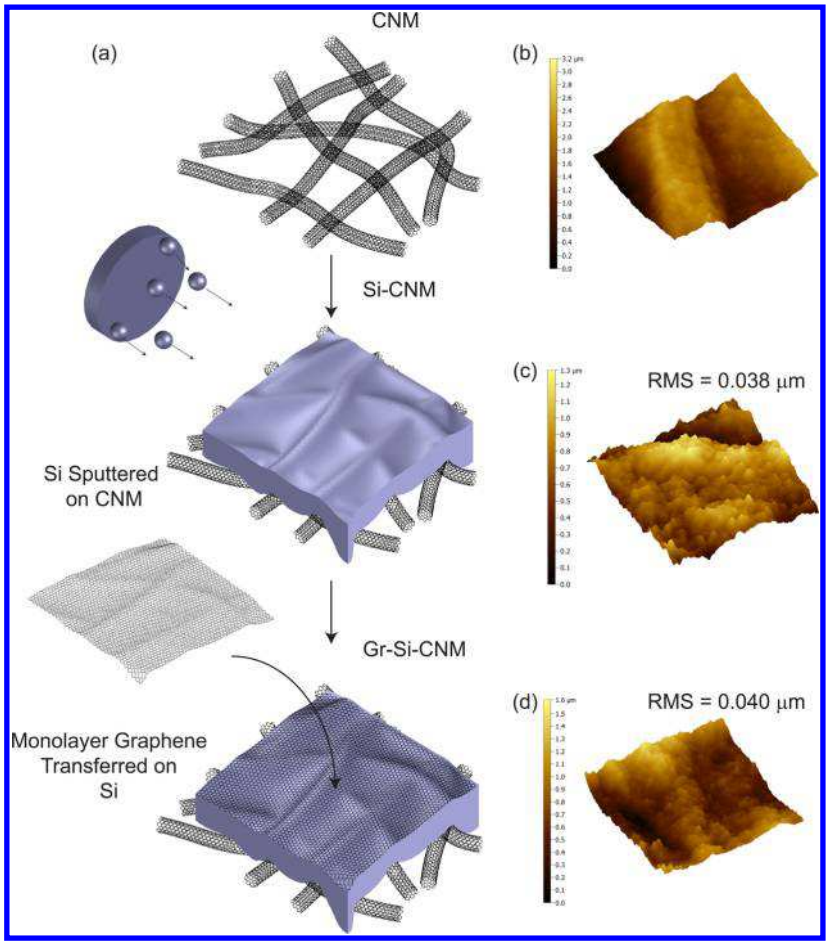

Figure 1. (a) Schematic representation of Gr-Si-CNM synthesis. Si was sputtered on a CNM film. A monolayer graphene sheet was then transferred onto Si-CNM by wet chemistry methods. (b–d) AFM images of CNM, Si-CNM, and Gr-Si-CNM. It can be seen that there are no appreciable differences in the RMS roughness of the Si-CNM and Gr-Si-CNM, indicating a conformal coating of monolayer graphene on Si after transfer.

based on the stoichiometry of the alloy $Li_{22}Si_5$) is ~10 times higher than graphite.[5] The quest for deploying Si anodes began over a decade ago by depositing bulk films of Si on metallic current collectors such as copper.[6] However, electrochemical and mechanical instabilities have plagued Si films and prevented its successful commercialization. Two fundamental reasons were identified as the root cause for failure of Si film anodes: (i) a volume expansion of ~300% in the lithiated state, leading to stress-induced pulverization and delamination of the brittle Si films, and (ii) an unstable solid electrolyte interface (SEI) layer for Si that leads to continual capacity fade with cycle index.[7] Due to these reasons, Si film anodes exhibit a rapid decay in capacity, culminating in complete failure, typically within less than 100 charge/discharge steps. As a consequence, the research community has over the years migrated away from bulk Si films toward different morphologies of nanostructured Si (*e.g.*, nanowires, nanotubes, and nanoparticles).[8,9] Indeed, such nanostructures have many advantages over bulk Si films. In addition to providing shorter Li-diffusion distances, it is widely established that nanostructured Si has superior resistance to fracture because cracks do not reach their critical size for propagation.[10] However, even for nanostructured Si, the unstable SEI problem persists, leading to capacity fade and limited cycle life. In a breakthrough, Cui's group has developed core–shell silicon–carbon nanoparticles with stable performance and a specific capacity of ~1500 mAh g^{-1} for 1000 cycles.[11,12] The core is composed of Si nanoparticles that are resistant to pulverization, while the carbon shell provides a stable SEI with the electrolyte. Later many such core–shell structures were designed using different forms of carbon, which have further validated this concept.[13−16] An alternative method for achieving a stable performance is by conformal coating of carbon materials on Si nanoparticles. Recently, Luo *et al.* demonstrated that with graphene-wrapped Si nanoparticles a capacity retention of ~668 mAh g^{-1} after 1300 cycles could be attained.[17] In another important study, the surfaces of Si nanoparticles were polymerized with polyaniline (PANi), and a specific capacity of ~1600 mAh g^{-1} was demonstrated after 1000 charge/discharge cycles.[18]

A review of the above literature indicates that every successful attempt at developing Si anodes with long cycle life has relied on the use of Si nanoparticles with some form of carbon coating or carbon shell. Such electrodes offer high performance but are more complex and expensive to manufacture. Further, the packing density of Si in its bulk form is the highest, and hence the volumetric energy density of porous Si nanoparticle based anodes is significantly lower than Si film anodes.[19] Therefore, if Si films could be rendered electrochemically and mechanically stable in a Li-ion battery environment, then this can offer significant benefit for practical applications. To the best of our knowledge, there is no report so far in the literature that demonstrates stable performance

DOI: 10.1021/acsnano.7b01780
ACS Nano 2017, 11, 5051–5061

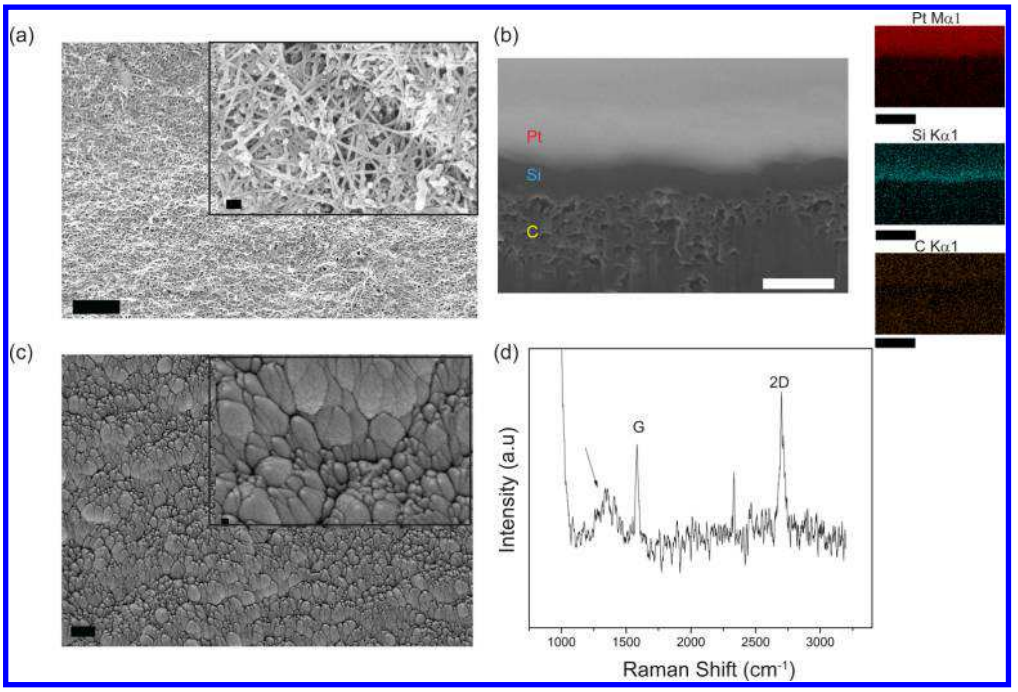

Figure 2. Characterization by scanning electron microscopy (SEM) and Raman spectroscopy. (a) SEM image of a carbon nanotube macrofilm (CNM). Inset shows a porous cross-linked network of nanotubes present in the CNM. The cross-linked carbon nanotube network endows high flexibility to the CNM. (b) FIB cross-section image of Si sputtered on CNM. The cross-section image shows a film-like morphology of Si deposited on CNM (Pt is deposited by FIB to improve cross-section surface quality). (c) SEM top view of Si sputtered on CNM. The roughness of the CNM substrate and internal pressure during the deposition create a cone-shaped surface texture. (d) Raman spectrum of Gr-Si-CNM confirming the presence of the graphene drape. A bump at around 1200−1500 cm^{-1} (indicated by the arrow) might be due to remnant PMMA introduced during the transfer. The scale bar in (a) is 2 μm, (b) is 500 nm, (c) is 1 μm. The scale bar in the insets of (a) is 200 nm, (b) (the EDS images) is 1 μm, and (c) is 200 nm.

and long life of several 100 nm thick Si films in a Li-ion battery setting. Here we demonstrate that such an outcome is possible, by concurrently implementing two strategies, *viz.*, using a carbon nanotube macrofilm (CNM) instead of copper as the current collector substrate and by draping the Si film with an atomically thin (*i.e.*, monolayer) sheet of graphene. The CNM substrate is highly flexible and allows the Si film to expand and contract during lithiation/delithiation cycles. This serves to "unconstrain" the Si film and minimizes stress buildup. The role of the monolayer graphene drape is to stabilize the SEI layer that is formed at the Si−electrolyte interface. When the Si film strains, the graphene layer will "slip" with respect to the Si, since there is a relatively weak van der Waals interaction between graphene and Si. Consequently, the underlying Si film is allowed to expand and contract without straining the mechanically fragile SEI layer, thereby leaving it intact.

The graphene capping sheet also functions as an interconnecting elastic web that helps to toughen the Si film and reduces its tendency to pulverize and delaminate. This is remarkable considering that the Si films that we tested (~200 nm to ~2 μm thick) are between 588 and ~5880 times thicker than the graphene drape (~0.34 nm). We demonstrate that such Si films anchored on a CNM current collector and draped by an ultrathin graphene capping sheet can endow a long cycle life to the Si film of up to 1000 charge/discharge steps with an average specific capacity of ~806 mAh g^{-1}. While gravimetric performance parameters[20] are important in aerospace applications (such as unmanned aerial vehicles), where weight is a premium, for the vast majority of portable electronics (*e.g.*, wearables, smart watches, cell phones, tablet computers, laptops) and automotive applications, the volumetric capacity becomes crucial due to the limited volume available in such devices. The packing density of Si in bulk films is much higher compared to nanoparticle systems, and therefore it is no surprise that the volumetric capacity of the graphene-draped Si films in our study (~2821 mAh cm^{-3} averaged over 1000 charge/discharge steps; refer to Figure 3d) is between 2- and 5-fold higher than what has been reported in the literature[12,17,18] for Si nanoparticle electrodes.

RESULTS AND DISCUSSION

Electrode Synthesis and Characterization. Monolayer graphene draped Si films are schematically shown in Figure 1a. Si films of two different thicknesses (~200 nm and ~2 μm) were deposited on a carbon nanotube macrofilm substrate by DC sputtering. We chose the CNM over copper (Cu) foil current collectors since metal foils are relatively rigid, resulting in shear stress buildup at the Si−Cu interface, which causes delamination of the Si film.[21,22] By contrast, the cross-linked and porous nanotube network (Figure 2a) provides a highly flexible matrix that can accommodate the tensile elongation of Si during lithiation. The CNMs used in this study were synthesized using a scalable floating catalyst chemical vapor deposition method and are composed primarily of double-walled carbon nanotubes.[23] Figure 2b shows a focused ion beam (FIB) produced cross-sectional view of the interface of a 200 nm thick Si film deposited on CNM indicating a film-like morphology. The top-view scanning electron microscopy (SEM) image of the as-deposited Si film is shown in Figure 2c. The cone-shaped morphology on the surface of the Si film (Figure 2c) can be attributed to the roughness of the CNM substrate and internal stresses created during deposition.[21] Such

DOI: 10.1021/acsnano.7b01780
ACS Nano 2017, 11, 5051−5061

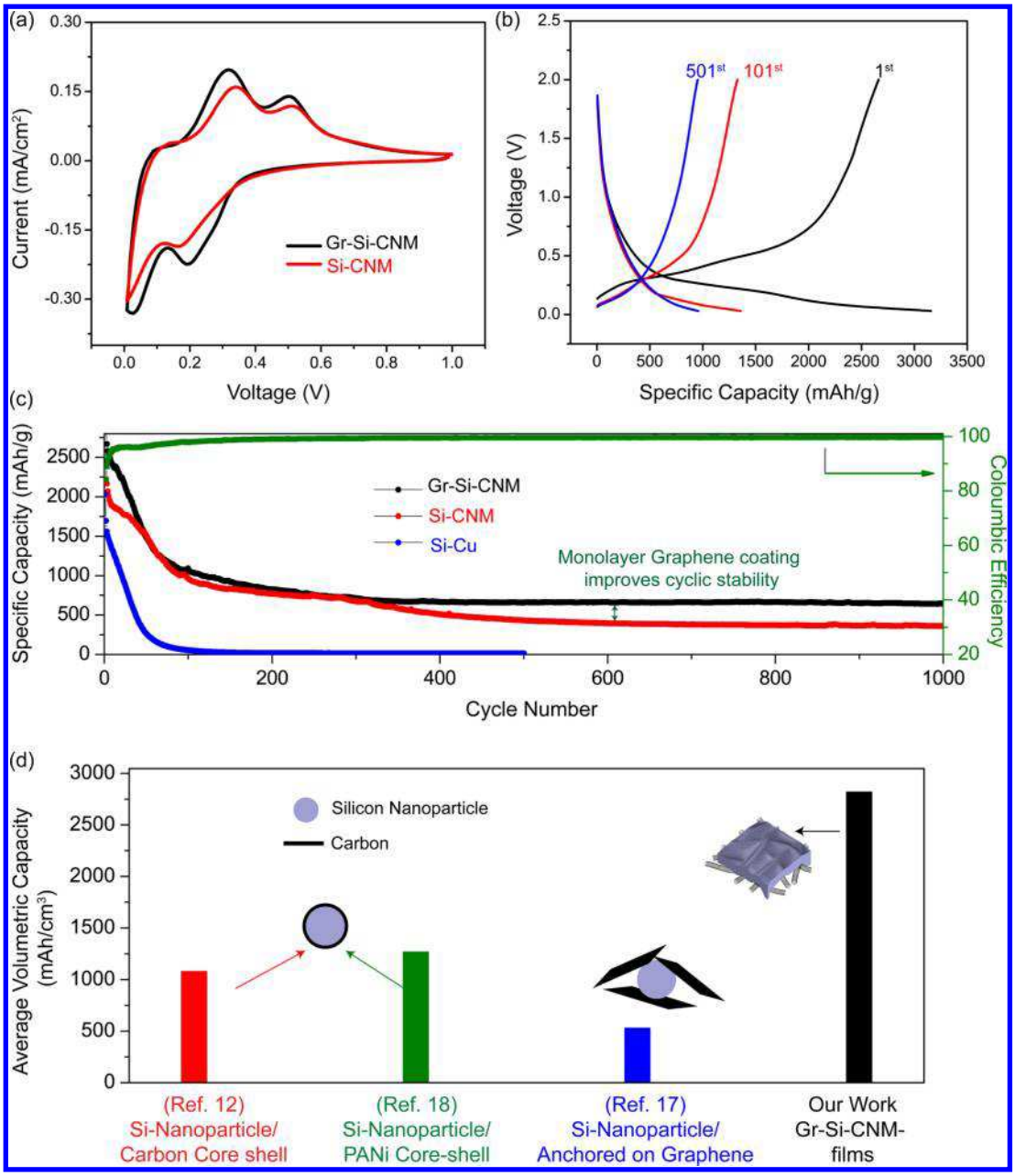

Figure 3. Electrochemical characterization of Gr-Si-CNM anodes with a 200 nm Si film. (a) Cyclic voltammograms (CVs) of Si-CNM and Gr-Si-CNM at a scan rate of 0.1 mV/s. The CV scans show that silicon is the active anode material in both Si-CNM and Gr-Si-CNM. (b) Galvanostatic charge/discharge curves of Gr-Si-CNM plotted after 1, 100, and 500 cycles. (c) Electrochemical cycling performance of Gr-Si-CNM, exhibiting a capacity of ~650 mAh g^{-1} and Coulombic efficiency of 99.67% after 1000 cycles at a current density of ~1.8 A g^{-1}. By contrast, the specific capacity of Si-CNM is much lower (~365 mAh g^{-1}) after 1000 cycles. Si films deposited on Cu foil (Si-Cu) exhibited a rapid decay and failed completely in less than 100 cycles. (d) Comparison of the volumetric capacity (averaged over 1000 charge/discharge cycles) of the Gr-Si-CNM anode with Si nanoparticle anodes (with carbon coating or core−shell structure).

amorphous Si films have been reported[24] to exhibit a modulus of ~95 GPa. A monolayer graphene sheet (Raman spectrum in Figure 2d shows the G and 2D band peaks) was draped on the Si film surface. The graphene sheets used in this study were grown on copper foils by chemical vapor deposition and then transferred onto the sputtered Si films by well-established wet chemistry transfer methods.[25] The presence of a symmetric 2D peak (with $I_G/I_{2D} \approx 0.5$) confirms that the graphene is predominantly monolayer.[26] The steps involved in synthesis of the Si film on the CNM current collector followed by draping of the Si film with the graphene sheet (Gr-Si-CNM) are illustrated in Figure 1a. Baseline Si films deposited on the CNM without the graphene coating (Si-CNM) and Si films deposited on conventional copper-foil current collectors (Si-Cu) were also synthesized and used as control samples to understand the role of the graphene coating. It can be seen from Figure 1b−d that the average roughness of Si-CNM and Gr-Si-CNM was ~0.038 and ~0.040 μm, respectively. This confirms that the graphene drape was highly conformal and covered the entire surface of the Si film.

Electrochemical Testing. Cyclic voltammograms (CVs) of Gr-Si-CNM and Si-CNM films with 200 nm Si film thickness were scanned in a voltage window of 0.01−1.5 V, as shown in Figure 3a. The anodic peak at ~0.2 V indicates the formation of

DOI: 10.1021/acsnano.7b01780
ACS Nano 2017, 11, 5051−5061

Li_xSi alloy in an amorphous Si (a-Si). The presence of two peaks in the anodic scan at ~0.30 and ~0.48 V corresponds to the delithiation reaction of Li_xSi transforming to a-Si. These peaks match well with the previously reported behaviors[27] of a-Si. It should be noted that the CV responses of Gr-Si-CNM and Si-CNM are very similar, which indicates that the graphene drape does not act as a barrier to the lithiation/delithiation of the underlying Si film. Lithium-ion diffusion into and out of the Si film presumably occurs through the defects and grain boundaries in the polycrystalline graphene.[28] We also observe in the CV curves of Gr-Si-CNM films that the peak current values are higher as compared to Si-CNM. We expect that this is because of structural changes to the SEI for Gr-Si-CNM, which improves the kinetics of the electrochemical reactions. Thus, the graphene drape augments only the interfacial charge transfer kinetics, but does not contribute to the charge storage capacity. This has also been corroborated by the voltage−capacity curves of Gr-Si-CNM half-cells, which exhibit a long plateau at ~0.19 V during lithiation and ~0.3 and ~0.5 V during delithiation, corresponding to a-Si. (Figure 3b). Further, we also confirm that due to the absence of any peak at ~0.1 V in the CV, the charge storage contribution of the CNM current collector is negligible.[29] This has been further validated by calculating the specific capacity of the bare CNM substrate (without Si), which was measured to be <50 mAh g^{-1} (Figure S1). Thus, from the CV and voltage−capacity curves, we conclude that Si is the major contributor to charge storage capacity and acts as the active anode material in both Si-CNM and Gr-Si-CNM films.

The cyclic stability of a 200 nm thick Si film on CNM capped with monolayer graphene (Gr-Si-CNM) is compared in Figure 3c with that of the two control samples, namely, the 200 nm Si film on CNM without the graphene capping layer (Si-CNM) and the 200 nm Si film on copper without the graphene capping sheet (Si−Cu). Figure 3c indicates that the Si film deposited on copper fails within few tens of charge/discharge cycles. By contrast, the Si film on CNM shows a marked improvement and exhibits a capacity of ~360 mAh g^{-1} after 1000 cycles. This we presume is because the Si film is allowed to expand and contract by the CNM current collector and is therefore far more resistant to delamination. However, the best performance was demonstrated by the Gr-Si-CNM anode with a specific capacity of ~962 mAh g^{-1} after the first 100 cycles. With further cycling, there was an additional capacity drop of ~25% until the 280th cycle. After 300 cycles, the capacity of Gr-Si-CNM remained quite stable at ~650 mAh g^{-1} up to 1000 cycles. The data shown in Figure 3c were obtained at an operating current density of 1.8 A g^{-1}. The Coulombic efficiency results for Gr-Si-CNM are included in Figure 3c and Figure S2. The cycling stability of Gr-Si-CNM was also investigated at current densities of 3 and 0.5 A g^{-1}. The first cycle discharge capacity at a current density of 3 and 0.5 A g^{-1} are ~2200 and ~3200 mAh g^{-1}, respectively (see Figure S3). Further, these samples were subjected to 300 cycles of charge/discharge (at current densities of 3 and 0.5 A g^{-1}), and the results from these samples (Figure S4) were consistent with the data shown in Figure 3c. It should be noted that although we see stable performance after 300 cycles, there is significant capacity fade in the first 100 to 200 cycles of charge/discharge. This initial capacity fade is presumably due to electrical disconnection of portions of the Si film from the CNM current collector surface (as shown schematically in Figure 5b). Despite the initial capacity fade, very high gravimetric (volumetric)

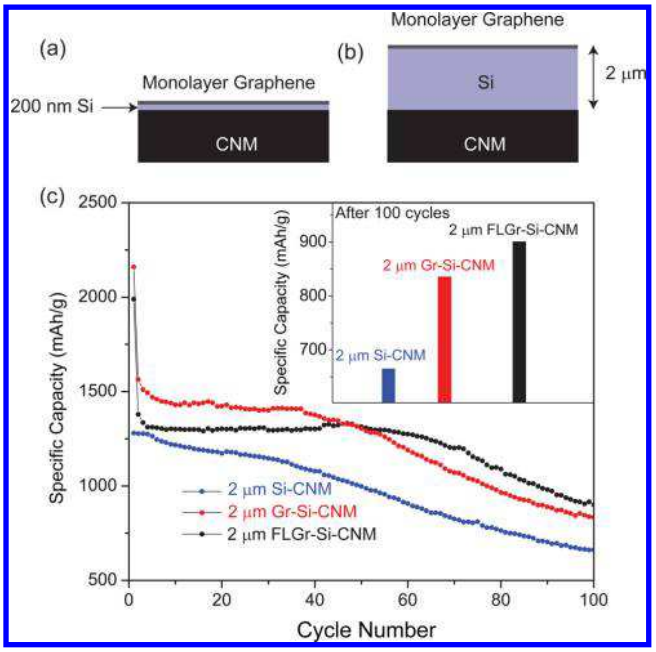

Figure 4. Scalability of Gr-Si-CNM electrodes. (a, b) Schematic representation of different thicknesses of Si in Gr-Si-CNM samples. The ~2 μm thick Si film corresponds to a mass loading of ~0.35 mg cm^{-2} compared to ~0.07 mg cm^{-2} for the ~200 nm thick film. (c) Electrochemical performance of a baseline 2 μm thick Si film on CNM without a graphene capping sheet (Si-CNM) and a 2 μm thick Si film on CNM with monolayer (Gr-Si-CNM) and a few layer graphene drape (FLGr-Si-CNM) at a current density of 3 A g^{-1}. Inset shows the comparison of specific capacity of Si-CNM, Gr-Si-CNM, and FLGr-Si-CNM after 100 charge/discharge cycles.

capacities of ~1290 mAh g^{-1} (~4500 mAh cm^{-3}) are achieved for the Si film anode over the first 200 cycles of charge/discharge, which decreases to ~806 mAh g^{-1} (~2821 mAh cm^{-3}) when the averaging is extended over 1000 charge/discharge steps.

We also demonstrate that the large initial capacity fade (in the first 100 cycles) can be significantly reduced by limiting the depth of discharge (DoD) from 100% to 80% as shown in Figure S5 (and also in Figure 6c). The Coulombic efficiency (after the initial few cycles) in our testing is >96% as indicated in Figure S2. The relatively lower Coulombic efficiency in the initial few cycles could be ascribed to local electrical disconnection of Si islands in some portions of the film, which results in the loss of Si and Li. The electrical disconnection can be suppressed by limiting the DoD; as shown in Figure S2, in the Gr-Si-CNM with 80% DoD, there is a significant improvement in the Coulombic efficiency during the initial 100 cycles. In this way, limiting the DoD not only reduces the rapid capacity decay in the initial cycles (Figure S5), but also improves Coulombic efficiency (Figure S2). Thus, through this study, we not only improved the cycle life of Si films but also designed densely packed Si films that possess a very high volumetric energy density. As indicated in Figure 3d, the average volumetric capacity of our Si films is ~2-to-5 times higher than previously reported Si nanoparticle (NP) based electrodes.[12,17,18] It should be noted that the volumetric capacity depends mainly on the density of Si (*i.e.*, the degree of close packing of the material). The densities of the Si-NP films used in the previous studies (Table S1 in the Supporting Information) are an order of magnitude lower than our Si films,

DOI: 10.1021/acsnano.7b01780
ACS Nano 2017, 11, 5051−5061

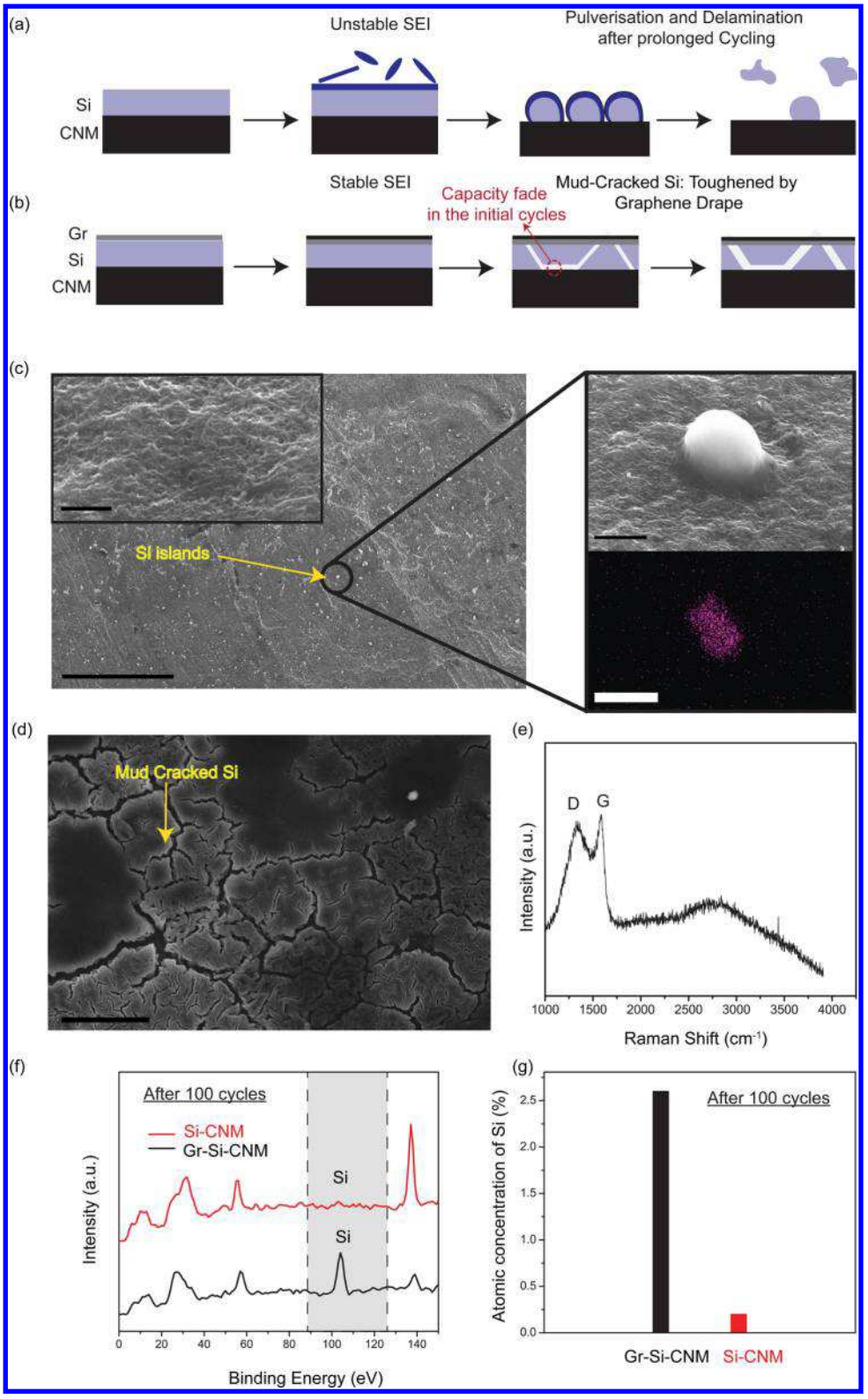

Figure 5. (a) Schematic representation of failure in Si-CNM electrodes due to unstable SEI and pulverization/delamination. (b) Schematic representation of the toughening mechanism of Gr-Si-CNM electrodes after prolonged cycling. (c) Postcycling SEM image of a typical Si-CNM electrode after 1000 charge/discharge cycles; Si has been almost completely delaminated from large portions of the CNM surface. Scale bar in the left image is 400 μm and in the inset is 500 nm. Scale bar in the right (top) image is 2 μm, and scale bar in the right (bottom) EDS image is 2.5 μm. (d) Postcycled SEM image of a typical Gr-Si-CNM sample after 1000 charge/discharge cycles. The toughened mud-cracked Si structure shows that graphene renders stability to the Si film. The scale bar is 40 μm. (e) Raman spectrum of a typical sample that has undergone 500 charge/discharge cycles indicating the presence of graphene after cycling. (f) XPS survey scan of Gr-Si-CNM and Si-CNM after 100 cycles, indicating that Si peaks are highly diminished in the Si-CNM, whereas a strong Si peak can be detected in the cycled Gr-Si-CNM. (g) Surface atomic concentration comparison of Si in Gr-Si-CNM and Si-CNM films. The surface concentration of Si in the Gr-Si-CNM sample is ~2.6% and is <0.3% in the Si-CNM.

DOI: 10.1021/acsnano.7b01780
ACS Nano 2017, 11, 5051−5061

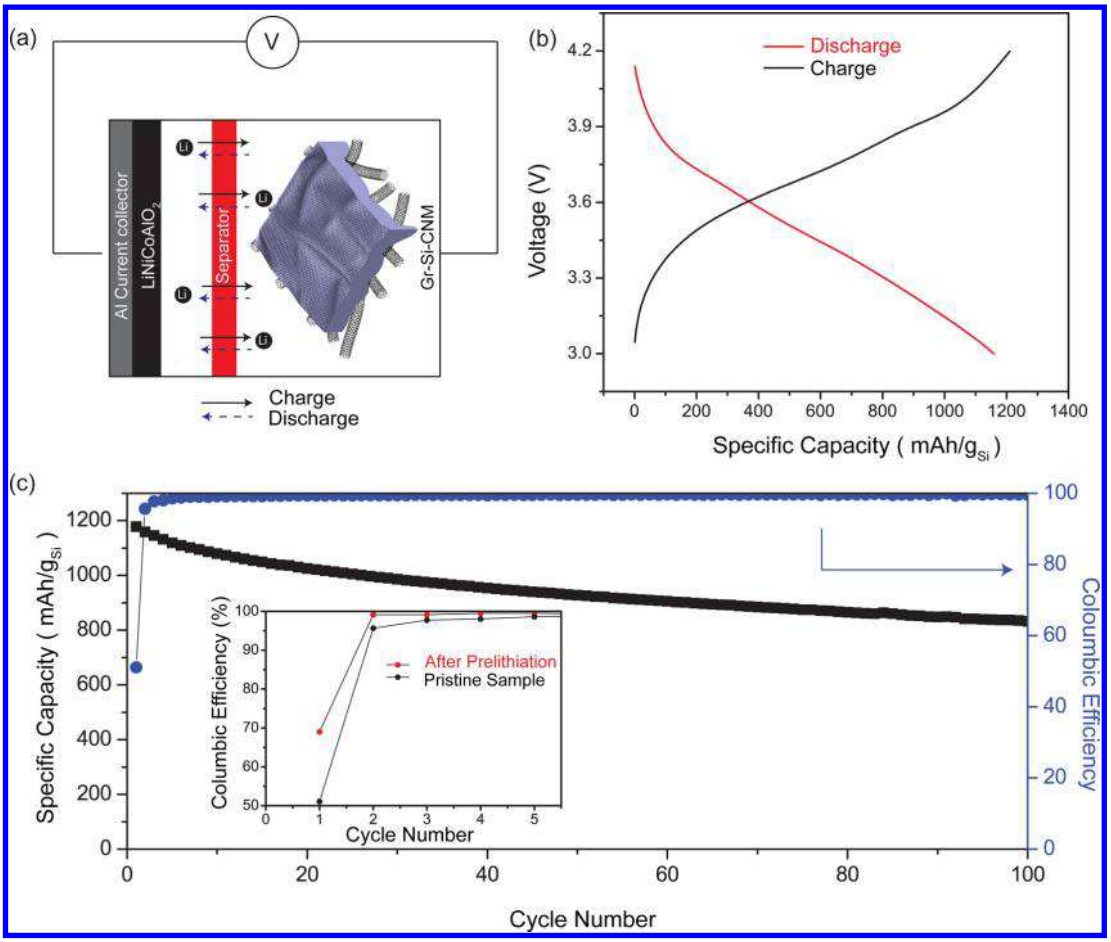

Figure 6. Electrochemical characterization of Al|NCA|Gr-Si-CNM full cell. (a) Schematic representation of the full-cell assembly in a 2032 coin cell using Gr-Si-CNM (with ~2.3 μm thick Si film) as the anode and commercially available $LiNiAlCoO_2$ as the cathode. The cells were operated at an 80% depth of discharge. (b) Galvanostatic charge/discharge curves of theAl|NCA|Gr-Si-CNM full cells plotted for the second cycle at a current density of ~0.5 A/g_{Si}. (c) Electrochemical cycling performance of the full cell, exhibiting a specific capacity of ~830 mAh/g_{Si} and a Coulombic efficiency of 99.63% after the completion of 100 cycles. Effect of prelithiation on the first-cycle Coulombic efficiency is shown in the inset.

which explains the relatively lower volumetric capacity of Si-NP-based electrodes. This higher density also means that in spite of lower overall thickness, the active material mass loading of our Gr-Si-CNM films (0.07–0.35 mg cm^{-2}) is of the same order as previously published work on Si-NP-based electrodes (Table S1 in the Supporting Information).

Having demonstrated improved electrochemical stability of Gr-Si-CNM with a 200 nm thick Si layer, we further extend this concept to higher mass loading (as shown schematically in Figure 4a,b). This was achieved by depositing thicker Si films (~2 μm in thickness, corresponding to a Si mass loading of ~0.35 mg cm^{-2} compared to ~0.07 mg cm^{-2} for the ~200 nm thick film). It should be noted that all the 2 μm thick Si films tested in Figure 4c are anchored on CNM current collectors and were cycled at a current density of 3 A g^{-1}. Consistent with our previous results for thinner Si films, the draping of the 2 μm thick Si with the graphene capping sheet significantly improves the capacity retention. The 2 μm Gr-Si-CNM film retained a specific capacity of ~835 mAh g^{-1} after 100 cycles at a current density of ~3 A g^{-1}. By contrast the 2 μm Si film on CNM without the graphene (Si-CNM) showed significantly greater capacity fade. We also investigated whether resorting to thicker graphene coatings (which can provide a stronger elastic web to suppress the pulverization and delamination of Si) is beneficial. To study this, we coated 2 μm thick Si films deposited on CNM with few-layer graphene (FLGr, 3–5 layer graphene). It was seen that the capacity retention improved to ~900 mAh g^{-1} after 100 charge/discharge cycles with the FLGr drape, as compared to ~835 $mAhg^{-1}$, with the monolayer graphene drape. Thus, we prove the effectiveness of graphene drapes on thicker Si films at higher mass loadings and demonstrate the viability of such coatings.

The toughening mechanism(s) for Gr-Si-CNM anodes are illustrated schematically in Figure 5a,b. In our electrode, the CNM current collector substrate plays a crucial role in managing the volume expansion of Si. The underlying CNM substrate is highly flexible[23] (with a modulus of <2 GPa (Figure S6), as compared to a reported[24] value of ~95 GPa for amorphous Si) and allows the Si film to expand and contract during lithiation/delithiation cycles. This "unconstrains" the Si film and minimizes stress buildup at the bottom interface. To demonstrate this, we have carried out molecular dynamics (MD) simulations (Figure S7) of lithiation of amorphous Si films. When unconstrained, there is no indication that lithiation causes fracture of Si (Figure S7a). By contrast, when we constrain the lower surface of the Si film (*i.e.*, prevent its ability to expand as in the case of Si deposited on a rigid metal current collector), it cracks and delaminates easily (see Figure S7b).

DOI: 10.1021/acsnano.7b01780
ACS Nano 2017, 11, 5051–5061

This brings out the critical role of the flexible CNM current collector in unconstraining the Si film. In spite of this, we recognize that local failure of the Si-CNM interface in some places (as shown schematically in Figure 5a,b) is unavoidable; the resulting electrical disconnection is the primary cause for the large capacity fade over the first 100−200 cycles of charge/discharge.

The top monolayer graphene capping sheet or drape also has an important role to play. When an amorphous Si film is fully lithiated, it expands by ∼300%. This strain is transferred to the SEI layer on the Si film surface. The SEI layer is mechanically fragile and is easily fractured when strained. Such fragmentation of the SEI layer that occurs repeatedly after every lithiation−delithiation step causes loss of Li and Si into the electrolyte (that is unrecoverable), leading to a continuous capacity fade with cycle index. The purpose of the top monolayer graphene capping sheet is to create a slippery van der Waals interface between the bulk Si film and the SEI passivation layer. Therefore, when the Si film expands by ∼300%, the graphene drape will "slip" with respect to the Si film, since there is a relatively weak van der Waals interaction between graphene and Si. As a result of this, the underlying Si film is allowed to expand "without" straining the SEI layer and thereby leaving it intact. This van der Waals slip phenomenon at the interface between the Si film and the graphene capping sheet is clearly observed in MD simulations as indicated in the Supplementary Figure S8.

The graphene capping layer also provides an interconnecting elastic web that toughens the Si film and reduces its tendency to pulverize and delaminate. The toughening effect of the graphene capping sheet was investigated by detailed *ex-situ* (*i.e.*, postcycling) characterization of the Gr-Si-CNM electrode. An intriguing observation for Si films (with graphene coating) in the postcycled state is that the structure resembles a toughened "mud-cracked" surface (Figure 5d) even after 1000 continuous charge/discharge cycles. On the other hand, large portions of the Si-CNM (without the graphene capping web) are completely delaminated with only discontinuous (isolated) Si islands present on the surface in the postcycled state (see energy dispersive X-ray spectroscopy (EDS) and SEM results in Figure 5c). This observation was also validated by surface concentration analysis using X-ray photoelectron spectroscopy (XPS) on Si-CNM and Gr-Si-CNM anodes that underwent 100 charge/discharge cycles (results in Figure 5f and g). The XPS spectrum (Figure 5f) indicates greatly diminished Si peaks in cycled Si-CNM with a surface concentration of <0.3% in contrast to a sharp Si signature with ∼2.6% Si in cycled Gr-Si-CNM anodes (Figure 5g). While cracking of Si films under prolonged cycling is unavoidable, the conformal graphene web that covers the Si film interconnects and cross-links the various regions of the Si film and considerably toughens it. This is akin to the role played by the fascia in the human body; the fascia is a band or sheet of connective tissue, primarily collagen, beneath the skin that attaches, stabilizes, encloses, and separates muscles and other internal organs. Similarly, it appears that in Gr-Si-CNM the conformal graphene web stabilizes the Si film and helps maintain its structural integrity. This is evident in the fact that a continuous Si film (albeit in a damaged mud-cracked state) is present on the current collector surface even after 1000 continuous charge and discharge cycles (Figure 5d).

To verify that the graphene capping layer is present on the surface of the Si film after cycling, we analyzed the Raman spectrum of the surface of a Gr-Si-CNM film that was cycled 500 times. We found prominent D and G peaks (Figure 5e) corresponding to the presence of sp^2 carbons in graphene. By contrast, the graphene film before electrochemical cycling did not exhibit a pronounced D peak (Figure 2d). Thus, the presence of a significant D peak (I_D/I_G ratio ∼1) and the absence of a 2D peak in the Raman spectra indicate that the graphene capping layer is now defective[26] and has been considerably damaged by the electrochemical cycling, but it is still intact and present on the Si surface.

To investigate the feasibility of deploying the Gr-Si-CNM in a full-cell configuration, electrochemical testing of full cells (shown schematically in Figure 6a) was performed. The Gr-Si-CNM anode was cycled in a full cell against commercially available $LiNiAlCoO_2$ (NCA) as the cathode to evaluate its cyclic stability. A Gr-Si-CNM (with ∼2.3 μm thick Si film) was used as the anode in order to balance the electrode capacities (NCA, capacity ∼200 mAh g^{-1} with a mass loading of ∼2.5 mg cm^{-2}, and Gr-Si-CNM, average capacity of ∼950 mAh g^{-1} with a mass loading of ∼0.4 mg cm^{-2}). The full cells were cycled at an 80% DoD, which limits the Gr-Si-CNM's specific capacity to ∼950 mAh g^{-1}. Operation at 80% DoD reduces stress buildup in the electrode and considerably mitigates the capacity fade. Note that commercial batteries are typically operated[1,28] at 50−80% DoD (∼50% in electric vehicles and ∼80% in consumer electronics), and so the DoD selected in our tests is consistent with industry standards. The voltage−capacity curve (Figure 6b) indicates a long plateau at ∼3.6 V, which is the nominal voltage of the NCA cathode. The cycle life curve of the full cell (Figure 6c) indicates a relatively stable performance with capacity retention of ∼75% after 100 charge/discharge cycles. In Figure 6b,c, the absolute capacity of the full cell is normalized by the Si mass. The corresponding areal capacity (*i.e.*, normalization by electrode area) results are provided in Supplementary Figures S9 and S10. The first cycle Coulombic efficiency in the full-cell test was relatively poor (∼50%). To address this issue, we employed a prelithiation strategy[28] where the Li lost during the first cycle (SEI and trapped charges) is compensated by Li from the prelithiation charge. To achieve the prelithiation, a Li metal foil was shorted[28] to the Gr-Si-CNM electrode. The effect of prelithiation has been shown in the inset of Figure 6c, where the first cycle Coulombic efficiency of the full cell has increased from ∼50% to ∼70%, which is consistent with industrial standards.[1]

CONCLUSIONS

To summarize, we have demonstrated a solution to better stabilize Si film anodes in Li-ion batteries. We compared the performance of our electrode with the best available Si technology, and the results are summarized in Figure 3d. It is evident that the only viable Si technology that can provide stable performance over a thousand charge−discharge cycles is comprised of either Si nanoparticles in core−shell form (with an encapsulating carbon shell)[12] or Si nanoparticles that are functionalized with carbon coatings.[17,18] In this work, we demonstrate that Si films can be engineered to rival this performance. Unlike the Si nanoparticles that have undergone complex modifications, the deposition of Si films is scalable and compliant with the process flow of semiconductor manufacturing industries. Another major advantage of silicon films is that they offer significantly higher volumetric capacity as compared to porous nanoparticle based electrodes. Figure 3d indicates that the volumetric capacity for the Gr-Si-CNM electrode averaged over 1000 charge and discharge steps is ∼2821 mAh cm^{-3}; this is about a factor of 2 to 5 times larger than Si

DOI: 10.1021/acsnano.7b01780
ACS Nano 2017, 11, 5051−5061

nanoparticle based electrodes.[12,17,18] As the mass loading (*i.e.*, thickness) of the Si film is further increased to meet industrial standards, it is likely that the monolayer graphene capping layer alone may not be sufficient. Such thicker Si films could possibly be stabilized by increasing the thickness of the graphene drape or by designing a structure with alternate stacks of Si films and graphene drapes, which would necessitate a layer-by-layer deposition strategy. Regardless, this work shows the extraordinary potential of atomically thin graphene drapes and CNM current collectors to counteract the mechanical and electrochemical instabilities that have so far prevented the successful commercialization of Si film technology in lithium-ion batteries.

MATERIALS AND METHODS

Synthesis of Carbon Nanotube Macrofilms. Carbon nanotube macrofilms were synthesized by a methanol-mediated floating catalyst chemical vapor deposition (FCCVD) method at 1150 °C, as reported in our previous work.[23] In a typical synthesis, CNMs of about ∼2000 cm^2 could be synthesized. The typical mass loadings of these current collector films were 0.6−0.8 mg cm^{-2} for a thickness of ∼3 μm.

Deposition of Silicon Films. Silicon was deposited on CNMs by DC sputtering in an AJA sputter system. An N-type silicon (Plasmaterials Inc.) target (∼2 cm in diameter) was used. The base pressure of the chamber was ∼1 × 10^{-7} Torr, and the working pressure was 3 mTorr. Silicon films of ∼200 nm and ∼2 μm were deposited at the same power by varying the deposition time. On these Si films, a monolayer graphene sheet was transferred by the wet-chemistry method.[25] The mass loadings of Si in 200 nm and 2 μm Si films were ∼0.07 and ∼0.35 mg cm^{-2}, respectively. The weight ratio of Si:C for 200 nm Si is ∼10%, and for 2 μm Si it is ∼50%.

Graphene Synthesis and Transfer. Monolayer graphene was grown by a chemical vapor deposition (CVD) process as reported previously.[25] In a typical synthesis, a ∼25 μm thick copper foil (99.99% Pure, Sigma-Aldrich) was used for the CVD graphene growth in a three-zone split-tube furnace. The deposition pressures of ∼1 Torr at 1020 °C with methane (CH_4) and hydrogen (H_2) flow rates (CH_4, H_2: 140, 10 sccm, respectively) were optimized to achieve a C:H ratio of 10:1. The as-grown monolayer graphene was transferred on Si-CNM by wet chemistry transfer methods.[25] The graphene on Cu foil was spin coated with poly(methyl methacrylate) (PMMA) at 2000 rpm for 20 s. After drying, the back side of this foil was then exposed to oxygen plasma at 50 W for 2 min to remove graphene. This foil was then immersed in a ∼0.25 M ammonium persulfate solution to etch Cu. The graphene-PMMA films were then carefully scooped onto Si-CNM and heated at ∼150 °C for ∼15 min to remove the excess water and soft bake PMMA. Finally, PMMA was stripped off from the surface by dipping it in acetone for ∼3 h at room temperature.

Structural Characterization and Raman Spectroscopy. Scanning electron microscope images of the Si films were acquired using a Zeiss Supra 55 FESEM at 2 kV. A Veeco Dimension 3100 was used to obtain the atomic force microscope (AFM) images. Tapping mode AFM scans were performed in an area of 20 × 20 μm on CNM, Si-CNM, and Gr-Si-CNM samples. A Renishaw Raman Scope 2000 equipped with a 514 nm laser and a 50× objective was used to measure the Raman spectrum of the as-grown graphene samples. An FEI Helios Nanolab 600i dual-beam FE-SEM/ion beam was used to image the electrode surfaces. Electron beam imaging was conducted with a beam voltage between 10 and 20 kV. For FIB cross-sectioning, the Ga^+ ion beam was operated at 30 kV at various beam currents.

Electrochemical Testing. The as-synthesized Gr-Si-CNM and Si-CNM films were tested as an anode in a 2032 type coin cell inside a glovebox (MBraun Labstar) with an oxygen and moisture content of <1 ppm. Lithium foils were used as a counter electrode, and a Celgard 2340 polypropylene membrane was used as the separator. A 1 M LiPF6 in a 1:1 mixture of ethylene carbonate and diethyl carbonate was used as the electrolyte. The lithium metal foil and electrolyte were purchased from MTI Corp. and Sigma-Aldrich, respectively. An Arbin BT2000 battery tester was used to perform the charge/discharge tests, and a potentiostat (Gamry Instruments Inc.) was used to obtain the cyclic voltammograms.

Disassembly of the Coin Cells. The coin cells with Si and Gr-Si-CNM samples were disassembled after 100, 500, and 1000 cycles in the glovebox for structural characterizations and SEM imaging. The samples retrieved from the coin cells were then washed with acetonitrile to remove the remnant electrolyte and were then dried overnight in the glovebox.

Scanning Electron Microscopy and Focused Ion Beam Cross-Sectioning Post Electrochemical Cycling. An FEI Helios Nanolab 600i dual-beam FE-SEM/ion beam was used to image the electrode surfaces after cycling. Energy-dispersive X-ray spectroscopy (EDS) was conducted using an Oxford Instruments X-MaxN detector and analyzed using Aztec 3.1 software. Spectra were collected using a 20 kV electron beam.

Raman Spectroscopy Post Electrochemical Cycling. To investigate the presence of the graphene drape, a small island was removed from the surface of the Gr-Si-CNM film that was cycled 500 times. A Raman microscope (100× objective and 100 μm optical fiber) with a conformal pinhole was used to acquire the Raman spectrum of this island.

X-ray Photoelectron Spectroscopy Post Electrochemical Cycling. The surface concentration was analyzed by a PHI 5400 X-ray photoelectron spectrometer equipped with a monochromatic Al Kα source (λ = 1486.7 eV). A detector pass energy of 23.5 eV and the sample to detector take off angle of 45° was used. The 284.8 eV C 1s peak was used for charging corrections. Films of 200 nm thick Si and Gr-Si-CNM, which underwent 100 charge/discharge cycles, were used for XPS analysis.

Molecular Dynamics Simulations. To simulate the lithiation process in amorphous silicon, we employ MD simulation with the ReaxFF potential developed for Li-Si systems by Jung and co-workers.[30] The total system energy is the sum of contributions from the electron lone pairs, overcoordination, undercoordination, valence and torsion angles, conjugation, hydrogen bonding, and van der Waals and Coulomb interactions.[31] This force field has been successfully used to determine the mechanical properties of amorphous alloys.[32] For simplicity, the interaction between carbon and lithium/silicon is modeled using a very weak Lennard-Jones potential. The 12−6 Lennard-Jones potential ($V(r)$) for two nonbonded atoms[33] is given by $V(r) = -Ar^{-6} + Br^{-12}$, where A and B denote the attractive and repulsive Hamaker constants, respectively. From the work by Chan and co-workers,[34] we choose an A value of 3.959 eV Å^6 and repulsive constant B of 904.438 eV Å^{12}, respectively. The carbon−carbon interaction in graphene is described by the adaptive intermolecular reactive bond order (AIREBO) potential.[35] Using this approach, we perform MD simulation to investigate lithiation in a-Si. We used the LAMMPS software, with a Verlet integration time step of 1 femtosecond. The atomic structure of a-Si is created by melting and subsequent quenching of single-crystal silicon. Both fully periodic a-Si and a-Si slab samples, the latter of which is periodic in the transverse directions and has two surfaces in the longitudinal direction, are prepared. The graphene sheet is sandwiched between a-Si samples, and the structure is equilibrated under a canonical NVT ensemble at 300 K. The lithiation process is carried out by deposition of lithium on a-Si samples with a driving force. First, a few lithium atoms are introduced in regions defined close to the two surfaces of the amorphous silicon. Then an external force of 10 kcal/mol-Å is applied to these lithium atoms to drive them into the a-Si system, in a process analogous to the voltage-driven lithiation of a-Si in an electrolytic cell. Finally, the freshly lithiated Li_xSi amorphous system (where the value of x depends on the degree of lithiation) is allowed to relax under NVT ensemble for ∼10 picoseconds. These steps are repeated to carry out lithiation to the desired extent, during which volume expansion of the initially amorphous silicon system is recorded and the relative slip of the graphene sheet is observed. Fracture in the Si film is detected when the relative distance between neighboring atoms exceeds the range of the Si potential. We also carried out grand-canonical Monte Carlo (GCMC) simulations to lithiate a-Si samples. Both the deposition

DOI: 10.1021/acsnano.7b01780
ACS Nano 2017, 11, 5051−5061

method (on a-Si slab samples) and the GCMC method (on periodic a-Si samples) provide very similar results. Due to ReaxFF being a relatively costly potential, the initial system size is limited to 1010 atoms. The temperature of 300 K is maintained by a Nose Hoover thermostat with a damping parameter of 0.01 fs^{-1}.

ASSOCIATED CONTENT

Supporting Information

The Supporting Information is available free of charge on the ACS Publications website at DOI: 10.1021/acsnano.7b01780.

Specific capacity of pure CNM current collector, Coulombic efficiency for Gr-Si-CNM electrode for different depths of discharge, first-cycle voltage profiles of Gr-Si-CNM at various current densities, specific capacity *vs* cycle index for Gr-Si-CNM electrode at various current densities, effect of depth of discharge on the capacity fade in the first 100 charge−discharge cycles, experimental results for tensile testing of the CNM current collector, MD simulations showing the effects of lithiation on a Si film with and without constraint, MD simulation showing interfacial slip at the interface between the Si film and the monolayer graphene capping sheet, voltage *vs* areal capacity results for Al/NCA/Gr-Si-CNM full cells, areal capacity *vs* cycle index for Al/NCA/Gr-Si-CNM full cells, and table showing comparison of electrode dimensions and volumetric capacities for Si nanoparticle based and Gr-Si-CNM electrodes (PDF)

AUTHOR INFORMATION

Corresponding Author

*E-mail (N. Koratkar): koratn@rpi.edu.

ORCID

Nikhil Koratkar: 0000-0002-4080-3786

Notes

The authors declare no competing financial interest.

ACKNOWLEDGMENTS

N.K. acknowledges funding support from the USA National Science Foundation (Awards 1435783, 1510828, and 1640340) and from the John A. Clark and Edward T. Crossan Endowed Chair Professorship at RPI. Z.W. acknowledges funding support from the National Natural Science Foundation of China (Awards 51202095 and 51264010). R.M. acknowledges funding support from the USA National Science Foundation (Award 1640340). The authors would also like to thank the staff of Rensselaer Polytechnic Institute Micro-Nano-Clean-Room (RPI MNCR) for their technical support.

REFERENCES

(1) Lithium-Ion Battery Market for Consumer Electronics, Automotive and Grid Energy & Industrial Application−Global Industry Analysis, Size, Share, Growth, Trends and Forecasts 2016−2026; *Transparency Market Report*, 2016.

(2) Teki, R.; Krishnan, R.; Parker, T. C.; Lu, T. M.; Kumta, P. N.; Koratkar, N. Nanostructured Silicon Anodes for Lithium Ion Rechargeable Batteries. *Small* **2009**, *5*, 2236−2242.

(3) Stephenson, T.; Li, Z.; Olsen, B.; Mitlin, D. Lithium Ion Battery Applications of Molybdenum Disulfide (MoS_2) Nanocomposites. *Energy Environ. Sci.* **2014**, *7*, 209−231.

(4) Kaskhedikar, N. A.; Maier, J. Lithium Storage in Carbon Nanostructures. *Adv. Mater.* **2009**, *21*, 2664−2680.

(5) Liang, B.; Liu, Y.; Xu, Y. Silicon-Based Materials as High Capacity Anodes for next Generation Lithium Ion Batteries. *J. Power Sources* **2014**, *267*, 469−490.

(6) Maranchi, J. P.; Hepp, A. F.; Kumta, P. N. High Capacity, Reversible Silicon Thin-Film Anodes for Lithium-Ion Batteries. *Electrochem. Solid-State Lett.* **2003**, *6*, A198−A201.

(7) Wu, H.; Cui, Y. Designing Nanostructured Si Anodes for High Energy Lithium Ion Batteries. *Nano Today* **2012**, *7*, 414−429.

(8) Sitinamaluwa, H.; Zhang, S.; Senadeera, W.; Will, G.; Yan, C. Carbon-Based Silicon Nanohybrid Anode Materials for Rechargeable Lithium Ion Batteries. *Mater. Technol.* **2016**, *31*, 1−12.

(9) Kim, H.; Lee, E.-J.; Sun, Y.-K. Recent Advances in the Si-Based Nanocomposite Materials as High Capacity Anode Materials for Lithium Ion Batteries. *Mater. Today* **2014**, *17*, 1−13.

(10) Kasavajjula, U.; Wang, C.; Appleby, A. J. Nano- and Bulk-Silicon-Based Insertion Anodes for Lithium-Ion Secondary Cells. *J. Power Sources* **2007**, *163*, 1003−1039.

(11) Liu, N.; Wu, H.; McDowell, M. T.; Yao, Y.; Wang, C. M.; Cui, Y. A Yolk-Shell Design for Stabilized and Scalable Li-Ion Battery Alloy Anodes. *Nano Lett.* **2012**, *12*, 3315−3321.

(12) Liu, N.; Lu, Z.; Zhao, J.; McDowell, M. T.; Lee, H.-W.; Zhao, W.; Cui, Y. A Pomegranate-Inspired Nanoscale Design for Large-Volume-Change Lithium Battery Anodes. *Nat. Nanotechnol.* **2014**, *9*, 187−192.

(13) Zhang, L.; Hao, W.; Wang, H.; Zhang, L.; Feng, X.; Zhang, Y.; Chen, W.; Pang, H.; Zheng, H. Porous Graphene Frame Supported Silicon@Graphitic Carbon *via In Situ* Solid-State Synthesis for High-Performance Lithium-Ion Anodes. *J. Mater. Chem. A* **2013**, *1*, 7601−7611.

(14) Yu, W.; Liu, C.; Hou, P.; Zhang, L.; Shan, X.; Li, F.; Cheng, H. Lithiation of Silicon Nanoparticles Confined in Carbon Nanotubes. *ACS Nano* **2015**, *9*, 5063−5071.

(15) Zhou, J.; Qian, T.; Wang, M.; Xu, N.; Zhang, Q.; Li, Q.; Yan, C. Core−Shell Coating Silicon Anode Interfaces with Coordination Complex for Stable Lithium-Ion Batteries. *ACS Appl. Mater. Interfaces* **2016**, *8*, 5358−5365.

(16) Lu, C.; Fan, Y.; Li, H.; Yang, Y.; Tay, B. K.; Teo, E.; Zhang, Q. Core-Shell CNT-Ni-Si Nanowires as a High Performance Anode Material for Lithium Ion Batteries. *Carbon* **2013**, *63*, 54−60.

(17) Luo, Z.; Xiao, Q.; Lei, G.; Li, Z.; Tang, C. Si Nanoparticles/Graphene Composite Membrane for High Performance Silicon Anode in Lithium Ion Batteries. *Carbon* **2016**, *98*, 373−380.

(18) Wu, H.; Yu, G.; Pan, L.; Liu, N.; McDowell, M. T.; Bao, Z.; Cui, Y. Stable Li-Ion Battery Anodes by in-Situ Polymerization of Conducting Hydrogel to Conformally Coat Silicon Nanoparticles. *Nat. Commun.* **2013**, *4*, 1943.

(19) Son, I. H.; Park, J. H.; Kwon, S.; Park, S.; Rümmeli, M. H.; Bachmatiuk, A.; Song, H. J.; Ku, J.; Choi, J. W.; Choi, J.-M.; Doo, S.-G.; Chang, H. Silicon Carbide-Free Graphene Growth on Silicon for Lithium-Ion Battery with High Volumetric Energy Density. *Nat. Commun.* **2015**, *6*, 7393.

(20) Mukherjee, R.; Thomas, A. V.; Datta, D.; Singh, E.; Li, J.; Eksik, O.; Shenoy, V. B.; Koratkar, N. Defect-Induced Plating of Lithium Metal within Porous Graphene Networks. *Nat. Commun.* **2014**, *5*, 3710.

(21) Rong, J.; Masarapu, C.; Ni, J.; Zhang, Z.; Wei, B. Tandem Structure of Porous Silicon Film on Single-Walled Carbon Nanotube Macrofilms for Lithium-Ion Battery Applications. *ACS Nano* **2010**, *4*, 4683−4690.

(22) Maranchi, J. P.; Hepp, A. F.; Evans, A. G.; Nuhfer, N. T.; Kumta, P. N. Interfacial Properties of the a-Si/Cu:Active−Inactive Thin-Film Anode System for Lithium-Ion Batteries. *J. Electrochem. Soc.* **2006**, *153*, A1246−A1253.

(23) Li, L.; Wu, Z. P.; Sun, H.; Chen, D.; Gao, J.; Suresh, S.; Chow, P.; Singh, C. V.; Koratkar, N. A Foldable Lithium-Sulfur Battery. *ACS Nano* **2015**, *9*, 11342−11350.

(24) Shenoy, B.; Johari, P.; Qi, Y. Elastic Softening of Amorphous and Crystalline Li−Si Phases with Increasing Li Concentration: A First-Principles Study. *J. Power Sources* **2010**, *195*, 6825−6830.

DOI: 10.1021/acsnano.7b01780
ACS Nano 2017, 11, 5051−5061

(25) Rafiee, J.; Mi, X.; Gullapalli, H.; Thomas, A. V.; Yavari, F.; Shi, Y.; Ajayan, P. M.; Koratkar, N. A. Wetting Transparency of Graphene. *Nat. Mater.* **2012**, *11*, 217−222.
(26) Ferrari, A. C.; Meyer, J. C.; Scardaci, V.; Casiraghi, C.; Lazzeri, M.; Mauri, F.; Piscanec, S.; Jiang, D.; Novoselov, K. S.; Roth, S.; Geim, A. K. Raman Spectrum of Graphene and Graphene Layers. *Phys. Rev. Lett.* **2006**, *97*, 1−4.
(27) Krishnan, R.; Lu, T. M.; Koratkar, N. Functionally Strain-Graded Nanoscoops for High Power Li-Ion Battery Anodes. *Nano Lett.* **2011**, *11*, 377−384.
(28) Xiang, F.; Mukherjee, R.; Zhong, J.; Xia, Y.; Gu, N.; Yang, Z.; Koratkar, N. Scalable and Rapid Far Infrared Reduction of Graphene Oxide for High Performance Lithium Ion Batteries. *Energy Storage Mater.* **2015**, *1*, 9−16.
(29) Xiao, Q.; Fan, Y.; Wang, X.; Susantyoko, R. A.; Zhang, Q. A Multilayer Si/CNT Coaxial Nanofiber LIB Anode with a High Areal Capacity. *Energy Environ. Sci.* **2014**, *7*, 655−661.
(30) Jung, H.; Lee, M.; Yeo, B. C.; Lee, K. R.; Han, S. S. Atomistic Observation of the Lithiation and Delithiation Behaviors of Silicon Nanowires Using Reactive Molecular Dynamics Simulations. *J. Phys. Chem. C* **2015**, *119*, 3447−3455.
(31) Ostadhossein, A.; Cubuk, E. D.; Tritsaris, G. A.; Kaxiras, E.; Zhang, S.; van Duin, A. C. T. Stress Effects on the Initial Lithiation of Crystalline Silicon Nanowires: Reactive Molecular Dynamics Simulations Using ReaxFF. *Phys. Chem. Chem. Phys.* **2015**, *17*, 3832−3840.
(32) Fan, F.; Huang, S.; Yang, H.; Raju, M.; Datta, D.; Shenoy, V. B.; van Duin, A. C. T.; Zhang, S.; Zhu, T. Mechanical Properties of Amorphous Li_xSi Alloys: A Reactive Force Field Study. *Modell. Simul. Mater. Sci. Eng.* **2013**, *21*, 74002.
(33) Jones, J. E. On the Determination of Molecular Fields. −1. From the Variation of the Viscosity of a Gas with Temperature. *Proc. R. Soc. London, Ser. A* **1924**, *106*, 441−462.
(34) Chan, Y.; Hill, J. M. Lithium Ion Storage between Graphenes. *Nanoscale Res. Lett.* **2011**, *6*, 203−209.
(35) Stuart, S. J.; Tutein, A. B.; Harrison, J. A. A Reactive Potential for Hydrocarbons with Intermolecular Interactions. *J. Chem. Phys.* **2000**, *112*, 6472−6486.

DOI: 10.1021/acsnano.7b01780
ACS Nano 2017, 11, 5051−5061